



# The roles of leaf area index and albedo in vegetation induced temperature changes across China using modelling and observations

Na Dong<sup>1</sup> · Ming Luo<sup>2</sup> · Zhen Liu<sup>3,4</sup>  · Junying Sun<sup>5</sup> · Kailu Wu<sup>6</sup> · Hui Lin<sup>7</sup>

Received: 26 March 2020 / Accepted: 20 October 2021 / Published online: 30 October 2021  
© The Author(s), under exclusive licence to Springer-Verlag GmbH Germany, part of Springer Nature 2021

## Abstract

The biophysical effects of vegetation changes are important in determining future climate changes using climate model. However, compared to observations, model has biases in energy exchange between vegetation and the lower atmosphere modulated by leaf area index and albedo. In this study, land-use induced anthropogenic influences, estimated as the differences between present land-use and idealized natural vegetation, on near-surface temperature were investigated using a regional climate model. Results show that present land-use transitions over China brings a cooler summer and winter accompanied by reduced diurnal temperature ranges by 0.11 °C and 0.25 °C respectively, which are mainly determined by the overwhelming increased evaporation and latent heat flux in summer and reduced net radiation in winter. Three vegetation pairs (i.e., forest and cropland, grassland and cropland, grassland and forest) were selected using observational datasets to evaluate vegetation induced climatic impact without atmospheric feedbacks across various climatic regimes. Albedo led absorbed radiation plays a dominate role in middle to north region while both LAI and albedo are significant below 30° N for latitudinal temperature changes between cropland and forest transitions. Model results have inconsistencies with observations on temperature trends caused by vegetation pairs, indicating summer cropland and forest over southern China is the most sensitive to the atmosphere conditions and forest and grassland pair is the least. These findings demonstrate the heterogeneous biophysical effect of vegetation in different climate zones and imply that a region-oriented parameterization of vegetation types should be applied in the land surface model to reduce uncertainties in future climate prediction.

**Keywords** Leaf area index · Albedo · Modelling · Observation · Temperature change

## 1 Introduction

Human activities such as deforestation and agriculture can bring about far-reaching changes in land-use. The resultant changes in vegetation alter land surface biophysical properties such as surface albedo, and leaf area index (LAI). However, their influence on regional and global climate changes remains largely uncertain in the magnitude, let alone the underlying mechanism (Brovkin et al. 2013; Zhang and Liang 2018). Particularly, biases in the vegetation and climate interactive modelling would mislead the acknowledgment of the actual potential of vegetation in future climate mitigation. Models and observations are two common ways to explore the vegetation induced surface climate change and reveal the mechanism. Also, they serve a supplement for each other to make the results more robust. In this sense, a better evaluation of climate effects of vegetation conversion can be beneficial of reducing the uncertainty in future

✉ Zhen Liu  
zliu33@pusan.ac.kr

<sup>1</sup> School of Geospatial Engineering and Science, Sun Yat-Sen University, Zhuhai 519082, China

<sup>2</sup> School of Geography and Planning, Sun Yat-Sen University, Guangzhou 510275, China

<sup>3</sup> Center for Climate Physics, Institute for Basic Science, Busan 46241, Republic of Korea

<sup>4</sup> Pusan National University, Busan 46241, Republic of Korea

<sup>5</sup> COMAC Flight Test Center, Shanghai 201323, China

<sup>6</sup> Zhejiang Environmental Technology Co., Ltd, Hangzhou 310023, China

<sup>7</sup> School of Geography and Environment, Jiangxi Normal University, Nanchang 330022, China

climate modelling, which is rarely discussed in the previous studies.

The biophysical impacts of land-cover change on regional climate are generally driven by two processes, namely, albedo induced net radiation changes and heat flux partitioning between sensible heat flux (SHF) and latent heat flux (LHF) (Pitman et al. 2011). Albedo determines the reflected amount of incoming solar energy back to the atmosphere, while the absorbed energy by the surface are partitioned into SHF and LHF depending on the soil moisture and vegetation properties (Davin and de Noblet-Ducoudre 2010; Mahmood et al. 2014). However, large discrepancies exist in climate models in the representation of biophysical feedbacks between vegetation variation and atmospheric changes. For instance, some models showed that afforestation has an albedo-driven warming effect (De Noblet-Ducoudré et al. 2012; Zhang et al. 2009), while others displayed an evapotranspiration (ET) dominated cooling effect (Li et al. 2016; Zhu and Zeng 2015). On global scales, Zeng et al. (2017) found that the increased LAI and ET has contributed 70% of the global net cooling over the past 30 years using an Earth System Model. Besides, Li et al. (2016) suggested that the latitudinal temperature change due to deforestation is mainly influenced by background conditions, to a lesser extent by biophysical changes such as albedo and ET efficiency. Though several global models [Max Planck Institute Earth System Model (MPI-ESM), earth system model of intermediate complexity (EMIC)] have been used to validate the impact of vegetation changes and the background climate (Winckler et al. 2017; Li et al. 2016), it is difficult for regional models, such as Weather Research and Forecast (WRF) model, to distinguish local from non-local effect and to isolate the background climate impact. Zhu and Zeng (2017) argued that the accuracy of model parameterization for phenology and optical properties of vegetation could be improved by combining with observational analysis.

Observational studies mainly utilize both satellite products and local meteorological measurements to investigate the relationship between regional climate and vegetation changes. However, these results show wide variation in magnitude and even in sign. Some research reported that afforestation decreases the mean summer temperature in all tropical and boreal regions (Alkama and Cescatti 2016; Li et al. 2015) while other studies showed a warming effect over boreal areas caused by LAI induced surface albedo reduction and an evaporation-driven cooling in arid regions (Forzieri et al. 2017). By using flux net datasets, Guo et al. (2016) and Wang et al. (2016) both revealed that ET plays a very important role in cropland led cooling during summer in Yangtze River region. Peng et al. (2014) compared satellite-observed land surface temperature (LST) of planted forest to those of adjacent grassland or croplands and found afforestation would decrease daytime LST and increase

nighttime LST on average over China. The recent satellite space-for-time methods revealed that the cooling impacts, especially due to afforestation and cropland expansion, are determined by ET induced latent heat changes from either water loss of forest or the irrigation of cropland in tropical and subtropical regions (Zhao et al. 2017; Ge et al. 2019; Shen et al. 2019). Afforestation in mid-tropical and semiarid regions warms local temperature (Huang et al. 2018b; Shen et al. 2019) resulted from albedo changes but cools dry land during daytime in all seasons (Wang et al. 2018). Most studies demonstrated that afforestation warms nighttime temperature (Peng et al. 2014; Ma et al. 2017) while Zhang and Liang (2018) indicated that afforestation from grassland to forest has decreased LST in nighttime by 0.2 K, and deforestation to cropland has decreased LST in both daytime and nighttime. In latitudinal changes, afforestation tends to warm the local surface air north of 45° N, and deforestation leads to warming south of 35° N but with low confidence (Lee et al. 2011). In-situ station measurements showed that the latitude of 35.5° N is suggested as the transitional border in which deforestation leads to warming to the south and cooling to the north (Zhang et al. 2014).

Meteorological stations are sparse in rural areas, making it difficult to collect sufficient observations with a major natural vegetation covering. Satellite data typically has either high spatial or temporal resolution. Moreover, it does not measure the parameters of interest directly, and requires substantial data processing, which decreases the accuracy and efficiency in quantifying the local climate effects of land-cover changes (Alkama and Cescatti 2016). Therefore, empirical analysis is insufficient to describe the inner dynamic energy exchange and water balance of the biophysical processes, which requires a theory model and mechanism foundation to provide robust validation. However, most previous studies use either observation analysis or model simulation method, and paid little attention in their pros and cons in describing the regional biophysical interactions between vegetation and temperature changes. In this study, both regional modelling and local observation analysis are provided to comprehensively evaluate their differences in representing vegetation effects on regional temperature over China. Related research recently are listed in Table 1.

Over the last 20 years, the increases of forest and cropland over China account for 25% of the net leaf area increase globally, which would potentially impact the climate at regional and possibly global scales through vegetation-climate interaction (Chen et al. 2019). Understanding the impact of LAI and albedo changes is especially challenging over China because of its large latitudinal coverage and associated heterogeneous humidity and radiative intensity. This paper presents a comprehensive and intensive comparison of temperature responses to vegetation changes between observed analysis and regional climate modelling.

In addition, the impact of background states is explored from simulations. With regional numerical modelling, the climate impact of anthropogenic-induced land-use changes is examined by looking at the differences between simulations forced by the present and the idealized natural vegetation land-use. We select three typical vegetation conversions (i.e., forest to cropland, grassland to cropland, grassland to forest) over six climatic regimes to reveal relationships among LAI, albedo and near-surface temperature changes using both observation datasets and numerical simulations. The data, models and methodology are described in Sect. 2. Section 3 provides results and discussions about the impact of vegetation changes on climate, latitudinal variations of vegetation-climate interactions, and the source of differences between two methods. Key finding and conclusions are summarized in Sect. 4.

## 2 Methodology

### 2.1 Research area

China extends from 4° to 53° N and 73° to 135° E. The country contains various regions with distinctive humidity and temperature characteristics. Here, we divide China into seven sub-regions according to their climatic conditions provided by the Chinese Resource and Environment Data Cloud Platform (<http://www.resdc.cn/Default.aspx>, accessed on 10 June, 2019) based on Zhu et al. (1962) and Zhu (1931) (Fig. 1). They are the Northeast humid and semi-humid region (NEH), North humid and semi-humid region (NH), North semi-arid region (NA), Northwest arid region (NWA), North and central subtropical region (NCSH), South subtropical and tropical region (SSH), and Qinghai-Tibet Plateau region. We have no available observation data for

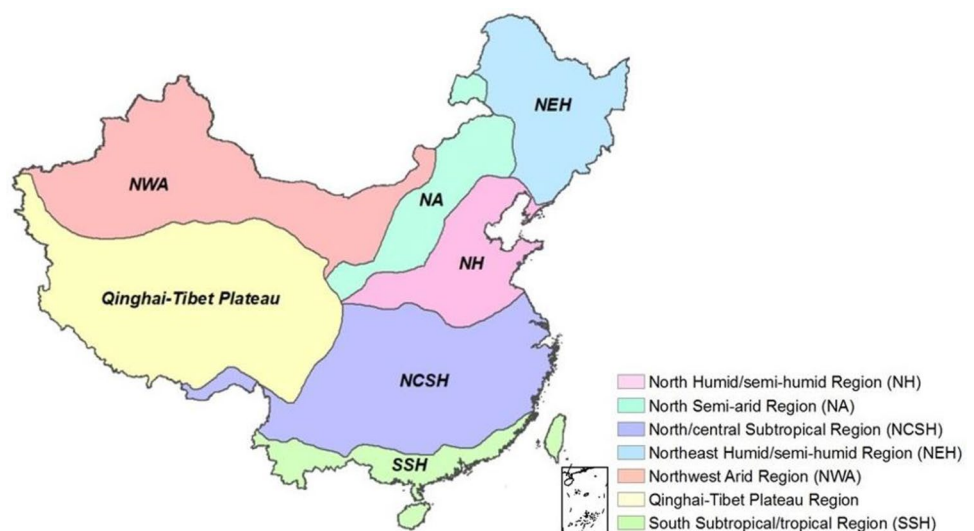
Taiwan, and the Qinghai-Tibet Plateau region exhibits complex topography and meteorological conditions, so we have excluded Taiwan and Qinghai-Tibet Plateau in this research. The boundaries and extents of each region are shown in Fig. 1.

### 2.2 Model and datasets

We integrate regional climate model outputs, satellite data and meteorological observations to analyse relationships between biogeophysical properties (e.g. albedo and LAI) and regional T2.

The Weather Research and Forecasting (WRF) model has been widely used in regional climate simulations (Argüeso et al. 2014; Chen and Frauenfeld 2016; Feng et al. 2012). In this study, WRF model (version 3.9.1; Skamarock et al. 2008) has been applied to perform regional numerical simulations. The initial and boundary conditions are based on the National Centres for Environmental Prediction (NCEP) FNL Final (FNL) Operational Global Analysis data (Research Data Archive at the National Centre for Atmospheric Research et al. 1999; <http://rda.ucar.edu/datasets/ds083.2/>, accessed on 3 November, 2019) achieved from the Global Forecast System (GFS) with a 6-h time interval at 1-degree resolution, which represents the current state of the climate conditions well. Meteorological datasets from 2474 Chinese in-situ stations and the Climate Research Unit Time Series (CRU TS) 3.2.1 dataset (Harris et al. 2014) (<https://crudata.uea.ac.uk/cru/data/hrg/>, accessed on 10 November, 2019) are adopted to validate the accuracy of the meteorological simulation of WRF (Fig. S1). The physical model configurations are the same as that used in Dong et al. (2019) and are listed in Table S1. Among those, the land surface scheme within WRF use the Noah Land Surface Model (Noah LSM; Chen and Dudhia 2001) with a single layer Urban Canopy

**Fig. 1** The distribution of regionalization over China in this study



Model (UCM; Kusaka and Kimura 2004), which simulates the energy balance and moisture exchanges between the surface and the lower atmosphere (Table 1).

Two land-cover datasets are used in this study (Fig. 2). The first group for the numerical simulation includes the potential vegetation (PVN) dataset and the Chinese Land-use Monitoring dataset (CLUM; Liu et al. 2010, 2014) 2000 (Fig. 2a, b). The PVN developed from the 5-min resolution dataset from Ramankutty and Foley (1999) is defined as undisturbed land surface condition (Findell et al. 2007) or preindustrial land-cover (De Noblet-Ducoudré et al. 2012) which provides a baseline to represent the natural development of land cover in the absence of human interventions. The contrast one to compare with PVN is the CLUM 2000 datasets with 1 km spatial resolution, which is considered as the land-use condition with anthropogenic impacts. The other group of datasets adopted in observational pair-site comparison is comprised of CLUM 2000, 2005, 2010, and 2015 which stand for different economic development levels

and thus display disparate proportions of land-cover types especially for urban with 1 km spatial resolution. PVN (Fig. 2a) differs in land classes from other CLUM datasets (Fig. 2b–e) which contain vegetation and urban land use types (Table. S2). The CLUM datasets are based on the dominant land type for each grid cell and exhibit a more scattered distribution than the PVN dataset. However, the land-cover classification scheme used in WRF are based on the MODIS classification scheme. To enable consistency between the PVN, CLUM and MODIS land-use systems, these datasets are harmonized using the reclassification rules shown in Table S2.

Besides, for observational comparison, monthly data for 2000, 2005, 2010, and 2015 on a 1 km grid of 10-daily albedo and LAI have been obtained from SPOT and PROBA satellite datasets through Copernicus Climate Data Store (<https://cds.climate.copernicus.eu/cdsapp#!/home>, accessed on 1 November, 2019). From the albedo dataset, white-sky albedos over the shortwave broadband is regarded as the

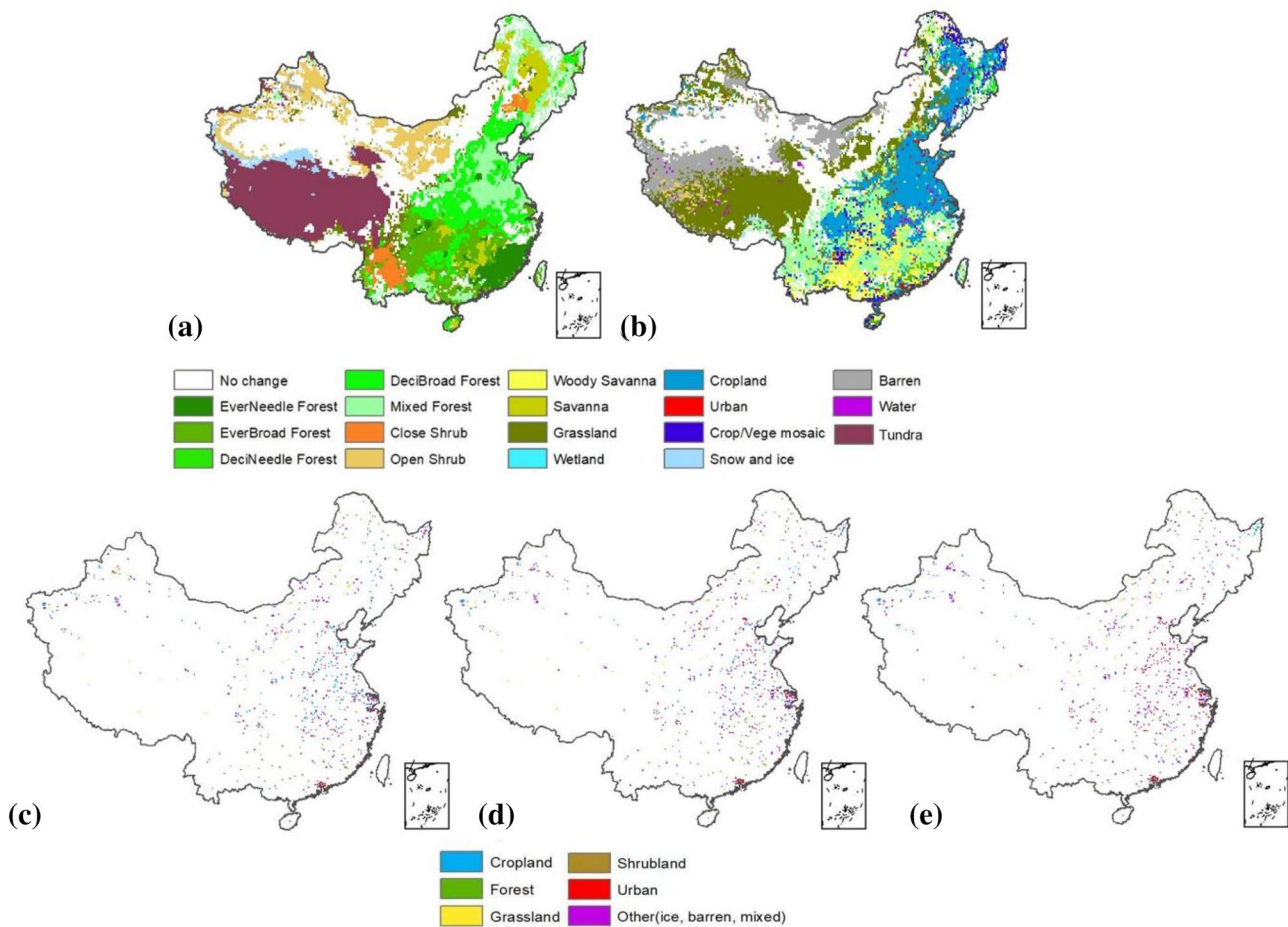


**Fig. 2** Overall spatial distributions of differences in the two groups of land-use/land-cover datasets. The differences of land-use/land-cover distributions used for WRF numerical simulations between: **a** potential vegetation and; **b** 2000 land-use in MODIS-based land-use clas-

sification; the differences of land-cover/land-cover distributions used for observational comparisons among: **c** 2005 land-use; **d** 2010 land-use; **e** 2015 land-use in 6 land-use classification which are resampled from 1 to 15 km for better presentation

**Table 1** Summary of recent research about vegetation change impact on global and regional temperature changes

Literature	Study area	Datasets	Land-cover type/changes	Temperature	Major conclusions
Ge et al. (2014)	Eastern China	WRF model	Vegetation increase and decrease	T2	Increased vegetation slows climate warming over North China Plain and southern China
Peng et al. (2014)	China	Satellite datasets	Forests, grasslands, croplands	LST	Afforestation decrease daytime LST and increase nighttime LST on average
Zhang et al. (2014)	Eastern Asia	Flux site	Forest, open land	T2	North of 10° N, forest warming increase with rising latitude
Guo et al. (2016)	Yangtze River valley of China	Meteorological and flux stations	Urban, suburban, grassland, farmland	T2, LST	Daily average T2 and LST between urban and crop has the largest differences which can be up to 3.21 °C and 7.26 °C
Ma et al. (2017)	China	Satellite datasets	Temperate forest, cropland	LST	Temperate forest to the south of 40° N showed cooling effect and presented warming effect to the north of 48° N
Zhao et al. (2017)	Northern China	Satellite datasets	Temperate semi-arid forest, cropland, grassland	LST	Cropland and planted forest tend to cool the
Wang et al. (2016)	Yangtze River Region	Meteorological and flux stations	Cropland, urban, grassland	LST, T2	LST by 5.15 and 1.51 °C during growing season compared to grassland
Cao et al. (2018)	China	WRF Model, satellite datasets	Land-cover change from 2001 to 2010	T2	Cropland cools LST while urban warms LST. Background climate reinforces land atmosphere feedback
Huang et al. (2018a)	China	Meteorological stations, satellite datasets, model	Afforestation, cropland expansion, urbanization	LST, T2	Extensive cooling in the Loess Plateau and northeastern China. Warming in Tibetan Plateau and Yunnan province
Huang et al. (2018b)	China	Meteorological stations, flux sites, satellite datasets	Forest, cropland, grassland	LST	Afforestation warm arid and semiarid regions, but cool subtropical zones. Cropland expansion is opposite to afforestation
Wang et al. (2018)	Kubuqi Desert, Inner Mongolia	Meteorological stations	Shrub and adjacent forest	LST, T2	Afforestation in dryland has a cooling effect in daytime and a warming effect in nighttime over all seasons except in summer
Zhang and Liang (2018)	China	Satellite datasets	Forest, crop, grassland	LST	Forest to cropland decreases LST because of albedo. Grassland to forest decreases LST due to ET changes
Ge et al. (2019)	China	Satellite datasets	Forest, adjacent open land	LST	Forest causes 0.23 °C through radiative effect and cooling through the non-radiative effect which explains about 79% of local LST

Table 1 (continued)

Literature	Study area	Datasets	Land-cover type/changes	Temperature	Major conclusions
Shen et al. (2019)	Guangdong	Satellite datasets	Natural forest, plantation forest, grassland, cropland	LST	Afforestation led to an overall cooling but had a warming effect in the mid-subtropical forest zone

independent status of the sky (Schaaf et al. 2002; Zhao and Jackson 2014) and used to calculate into monthly average to represent the surface albedo characteristics. Terrain data from the Shuttle Radar Topography Mission (SRTM) in 90 m has been upscaled to 1 km to match the spatial resolution of other datasets. Monthly average T2 temperature (T2-ave), maximum T2 temperature (T2-max), minimum T2 temperature (T2-min) during 2000–2015 have been extracted from the 1 km meteorological datasets published for China by Peng et al. (2019). All monthly variables are aggregated to seasonal mean (June, July, and August, JJA for summer; December, January, and February, DJF for winter) within the six climatic zones (NH, NA, NCSH, NEH, NWA, and SSH).

### 2.3 Experiments

Two groups of experiments, numerical climate simulations by WRF and observational pair-site comparison, are taken in this study (Table 2) to show land-cover impacts on local climate modulated by albedo and LAI changes. First, PVN and CLUM 2000 land-cover datasets are embedded into WRF through replacing its default static geographical data. In this way, LAI and albedo will be recalculated according to the indicated land-cover datasets in the WRF pre-processing. We implement the paired WRF model simulations with separate land-cover data from PVN and CLUM2000 forced by the same initial and boundary condition of the FNL analysis dataset from 2000 to 2010. The differences between two simulations are used to estimate how land-cover changes affect the biogeophysical processes through altering the energy exchange and water balance. The simulation with 2000 land-cover data is referred to as the control experiment named CTL\_2000\_LND\_2000 (CTL) while the other one with PVN land-cover data is indicated as NTR\_2000\_LND\_PVN (NTR). The major differences of these two land-cover data inputs are whether including the impact of human activities (i.e., CTL in Fig. 2b) or not (i.e., NTR in Fig. 2a), such as urbanization and agricultural development. As urbanization expansion in 2000 is still low over China, climate changes induced by vegetation nearby will not be considered as strongly affected by human activities. The model domain covers the whole China at a resolution of 20 km, and includes 253 grid points in the east–west direction and 214 grid points in the north–south direction. There were 36 vertical atmospheric levels up to 50 hPa. Both two experiments were integrated for 108 days in summer and 106 days in winter from 16<sup>th</sup> May to 1st September and 16th November to next 1st March respectively, for each year during 2000–2010. To reduce the internal noise and enhance modelling robustness, we conduct three ensemble simulations for each experiment by perturbing initial conditions starting at different time with an interval of 3 days.

**Table 2** The simulation and observational experiments designed in this research

Group	No.	Experiment name	Scenarios	Land-use/land cover datasets	Initial/boundary conditions	Experiment schemes
Simulation	1	NTR_2000_LND_PVN (NTR)	Natural land-cover without human intervention	Potential vegetation without urban and crop	NCEP FNL analysis data from 2000 to 2010	May 10th 2000–March 1st 2010 May 13th 2000–March 1st 2010 May 16th 2000–March 1st 2010
	2	CTL_2000_LND_2000 (CTL)	Control experiment under anthropogenic impact of 2000 land-use	CLUM 2000		May 10th 2000 – March 1st 2010 May 13th 2000–March 1st 2010 May 16th 2000–March 1st 2010
Observation	1	Observ_2000	Low economic development	CLUM 2000	Satellite products of the surface albedo, LAI and T2 from meteorological stations	Pair-sites are extracted within nearby 9×9 window for various land-use type of each year. The number of pair less than 10 in each zone are not considered
	2	Observ_2005	Moderate economic development	CLUM 2005		
	3	Observ_2010		CLUM 2010		
	4	Observ_2015	High economic development	CLUM 2015		

The simulation periods before 1st June and 1st December were treated as the spin-up time and not considered in the analysis. Then the anthropogenic land-use change effects on regional climate and energy exchange process are investigated by comparing the differences in albedo, LAI, ET, LHF, SHF, and T2 between two scenarios. The Student's-t-test is used to estimate the significance of changes in climatic variables.

Second, vegetation conversion pairs are extracted using pair-sites method based on CLUM land-cover datasets of 2000, 2005, 2010, and 2015 (Fig. 2b–e) which is also called space-for-time approach (Huang et al. 2018b; Chen and Dirmeyer 2020). Vegetation pixels within 5 pixels to urban pixels are excluded as urbanization would strongly contaminate vegetation induced climate change. To get more matched vegetation pair-sites and reduce the impact from surrounding land-cover types, each CLUM dataset is resampled to 5 km spatial resolution. A dominant land-use/land-cover type, with a contribution of 80% or more, is considered as the type of that area. If no dominant type can be found, this resampled pixel is marked as missing value. One exception is urban samples with a fraction of 40% as the threshold, which are used to filter vegetation extraction. Pair samples are searched for each land-cover type (forest, grassland, cropland, shrubland, urban) of each CLUM dataset. After multiple tests, the searching rules are based on a reference sample and its adjacent samples within a 9×9 window, which can fulfil both the closest distance and ensure enough amounts of sample pairs by multiple tests. For example, the surrounding 9×9 windows of each cropland sample are searched to choose its paired

land-cover types (i.e., forest). If there is more than one sample of the same type within the window, the values of these samples will be averaged, and then one cropland and forest (cropland-forest) pair-site is extracted. This method has been adopted by several researchers such as Li et al. (2015) and Ma et al. (2017). Besides, to eliminate the elevation impacts on paired land-cover climate, pair-sites with an elevation difference above 50 m are discarded. We focus on three land-cover vegetation pair-sites, including cropland-forest, forest-grassland, and cropland-grassland as shrubland and urban can hardly found enough paired pixels nearby (less than ten in each zone). An assumption is made that these pair-sites are shared with the same background climate as the actual distance between each site is less than 45 km. We further accordingly composite averaged monthly albedo, LAI from satellite observations, and T2-ave, T2-min, and T2-max from interpolated observed meteorological data based on paired vegetation samples. Comparisons of T2 in summer (JJA) and winter (DJF) are made between vegetation pairs among various climatic zones, as well as their relationship with albedo and LAI changes. Latitudinal temperature variations for each vegetation pair are also evaluated to examine possible climatic dependence on latitudinal distribution. Finally, correlations between modelling and observations are assessed for changes of summer and winter T2-ave for each vegetation pairs (forest-grassland, cropland-forest, cropland-grassland) in each zone. The modulation impact of background climate on the land–atmosphere flux exchange in response to vegetation types and surface property changes is also examined as background climate and land-cover change

are full coupled in the numerical simulations while separated for the pair-site observations.

### 3 Results and discussion

#### 3.1 Simulated climatic variations of natural and anthropogenic land-cover

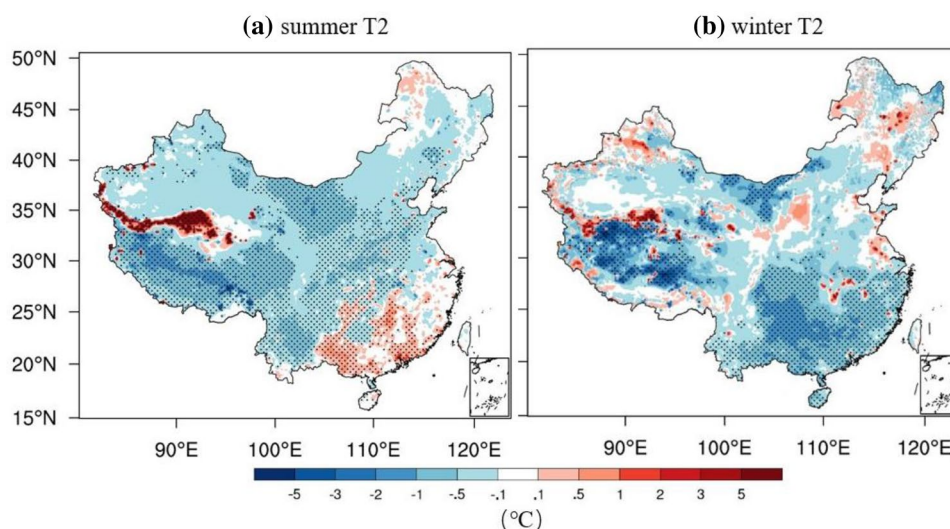
Compared to the CRU TS data and the interpolated climate data using in-situ meteorological stations, the WRF model well captures the pattern of temperature changes over China in spite of some underestimations during the winter season (Fig. S2).

Constrained by the same forcing of atmospheric boundary conditions and greenhouse gas (GHG) concentrations in 2000, the differences between the CTL and NTR simulations demonstrate remarkable T2 and P changes in response to vegetation conversions (Fig. 3). Excluding Qinghai-Tibet Plateau region, the area averaged climate changes show both cooling effects by 0.2 °C and 0.31 °C for summer and winter, respectively, in CTL compared to NTR. Stronger T2-max differences are found in CTL than NTR, with a small T2-max of 0.27 °C for summer and 0.45 °C for winter (Fig. S3). The diurnal temperature range (DTR) is reduced by 0.11 °C in summer and 0.25 °C in winter for CTL in comparison to NTR. The main land-cover transition from NTR and CLT is conversions from forests to croplands and grasslands which counts for 64% of the whole. These responses of temperature and DTR to deforestation changes are consistent with previous studies (De Noblet-Ducoudré et al. 2012; Xu et al. 2015) although with a relatively different magnitude, which may be induced by the different simulation resolution and land-cover data. T2 changes show an opposite sign between summer and winter over southern China and the

Northeast Plain but are consistent over North China Plain and Northwest regions (Fig. 3a). The increased summer T2 in CTL over southern China is mainly led by conversions of mixed forest to grassland while the decreased winter T2 over the Northeast Plain results from conversions of shrub and grassland to cropland. Most of the regions over the domain displays a lower temperature in NTR than that with present land-use condition, with a significance level of 0.05.

LAI changes in relation to the evaporation and humidity are also explored to further understand the temperature changes. As indicated in Figs. 4 and 5, CTL and NTR show distinct differences in the land properties of albedo, and LAI. These changes modulate energy partitioning (SHF and LHF) and water budget (ET) processes between the surface and the lower atmosphere. In CTL, obvious LAI increases appear over areas along the northeast to southwest line and the central China where deciduous broadleaf forests and savannas are converted to mixed forest and croplands; whereas, reductions are shown over areas in the transition of evergreen broadleaf and mixed forests to savannas and croplands and from tundra to the grasslands (Fig. 4a). This means that LAI even strongly varies within the forest type, for instance, mixed forest is lower than evergreen broadleaf forest but higher than deciduous broadleaf forest. Deforestation to croplands and savannas decreases the  $R_s$  higher than 1–0.4 (NCAR 2016), which plays dampening roles in adjusting ET and humidity. Humidity and ET changes are very similar and depend highly on local climate change and soil moisture. The increase of humidity in the north-eastern and central region and LAI in southwest region together leads to the increase of evaporation and reduction of summer T2 changes (Figs. 4b and 3a) in CTL. Inconsistent changes between decreased LAI and increased humidity over the middle-eastern China which presents major land-cover transitions from mixed forest to cropland, induce an increase of ET

**Fig. 3** Differences in **a** summer T2 and **b** winter T2 between the CTL and NTR. Regions with dots mean variations that have passed the significant t-tests ( $p < 0.05$ )





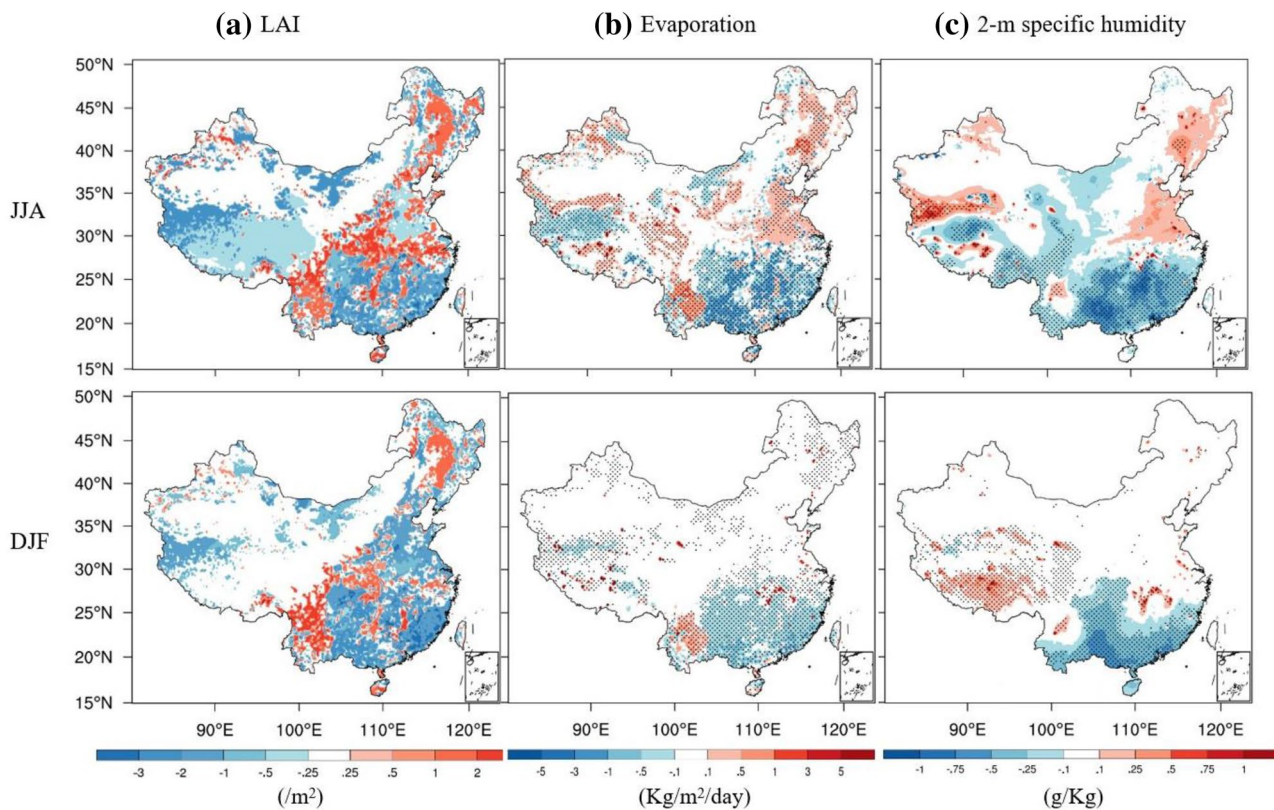


**Fig. 4** Same as Fig. 3 but for **a** LAI, **b** evapotranspiration (ET) and **c** 2-m specific humidity. Regions with dots mean variations that have passed the significant t-tests ( $p < 0.05$ )

and LHF in summer. With a small amount of precipitation and run-off in winter, ET decreases in southern China due to humidity reduction and slight increases in the southwest due to LAI rising (Fig. 4a–c).

Albedo increases in nearly all parts of China (Fig. 5a) except for the northeast and parts of southwest China in CTL, thus reducing the shortwave radiation at the surface and affecting the total energy available for both the SHF and LHF, i.e., the surface net radiation (Pielke et al. 2011). This is mainly seen over the regions of mixed forests, cropland and woody savannas which replace the former potential natural vegetation of evergreen broadleaf, evergreen needleleaf and deciduous broadleaf forests in NTR land-cover. Transitions from savannas and forests to croplands increase winter albedo over central and northeast China for CTL. Increased shortwave radiation driven by albedo variation are enhanced by the surface LHF loss over southern China, resulting in warmer climate and increased SHF during the summer (Fig. 5a–c). Other regions such as central, and Inner Mongolia demonstrate significant albedo increase, which overwhelms LHF reduction, leading to decreased T2 in summer. Though the stronger increases in LHF are partly counteracted by the increases in the absorbed net radiation over southwest and northeast region, T2 in those regions

still shows cooling trends. Albedo changes over the southern China in winter exhibit stronger signals to those in summer, thus overweighing the warming effect of LHF loss and making whole cooling climate to the southern China. The reduced albedo in central northeast China and Loess Plateau combined with the limited ET and precipitation increases the average T2 in winter. Northern region of China dominated by the increase albedo displays cool winter T2 to a large extent. Thus, Northeast China Plain and southern China are dominated by ET and LHF changes in summer and by albedo and SHF changes in winter. Centre China shows minor albedo changes from mixed forest to cropland, which is primarily affected by ET and LHF.

### 3.2 Observational temperature effects of different vegetation conversions

Using CLUM land-cover in 2000, 2005, 2010, and 2015, we generate the neighbouring land-cover pairs for forest, cropland, and grassland over the six zones (Fig. 6a). Totally, there are 1982 pairs of cropland–forest, 3643 pairs of cropland–grassland, and 808 pairs of forest–grassland samples within their surrounding  $9 \times 9$  window areas. With varying humidity and sunshine, each zone shows distinct

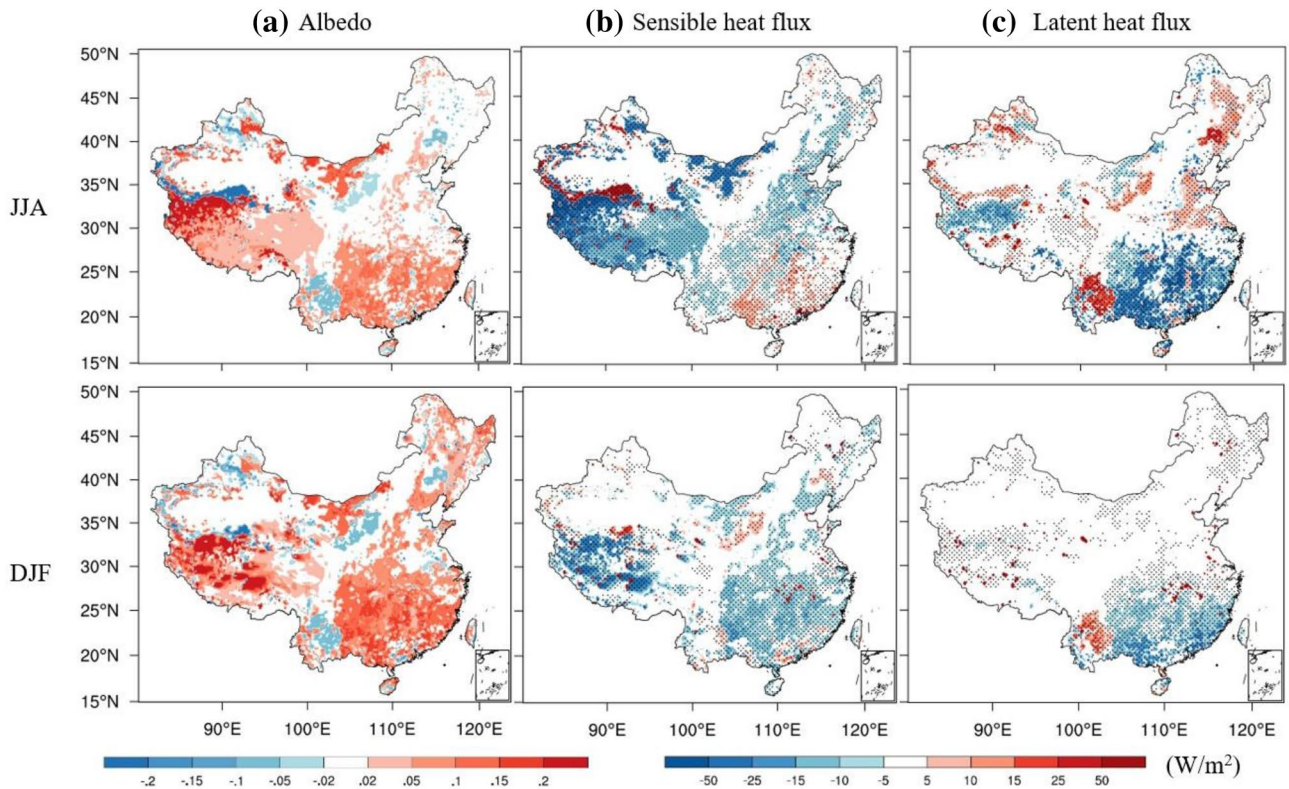


**Fig. 5** Same as Fig. 3 but for **a** albedo, **b** sensible heat flux (SHF), and **c** latent heat flux (LHF). Regions with dots mean variations that have passed the significant t-tests ( $p < 0.05$ )

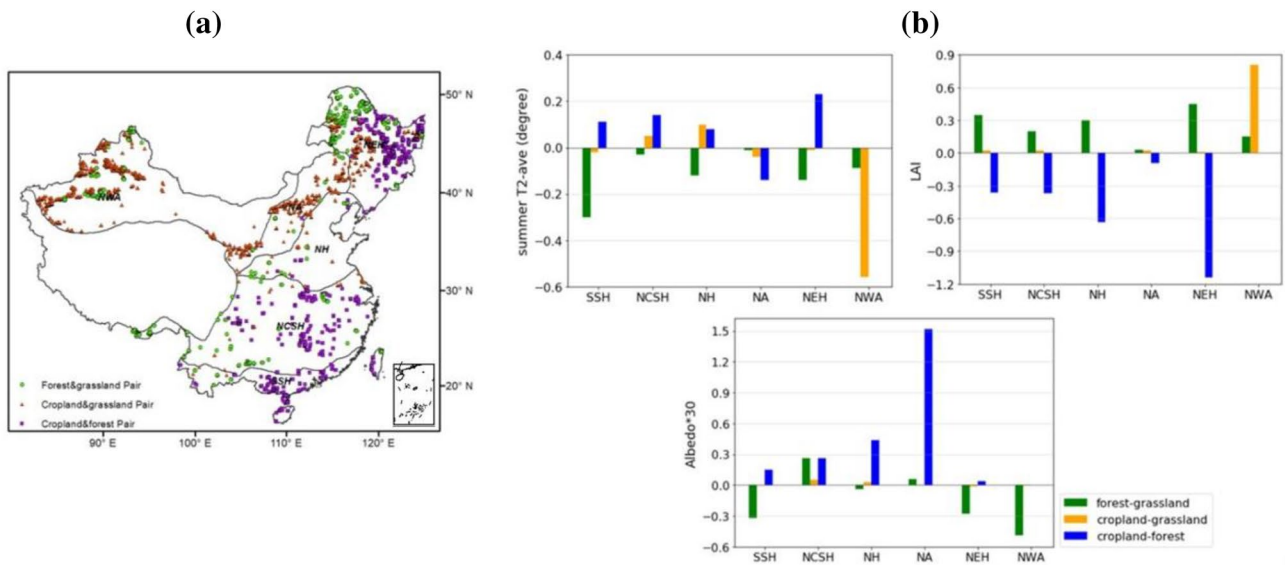


**Fig. 6 a** All vegetation conversion pairs within 9 km distance, including forest–grassland, cropland–grassland, and cropland–forest pairs in the years of 2000, 2005, 2010, and 2015; **b** areal averaged summer T2-ave, LAI, and albedo over SSH, NCSH, NH, NA, NEH, and NWA

for three types of vegetation conversions. Grids with 25 square kilometers are considered as a pure vegetation type when there are higher than 80% are the same type. To make the change obvious, we enlarge albedo by thirty times

characteristics of vegetation distribution. For instance, NEH is a northern temperate and semi-arid region with both moderate humidity and temperature and owns abundant pairs of all three types of land-cover pairs, while NH has the lowest number of vegetation conversion pairs as most NH areas are urbanized. The temperate and arid climate offer suitable conditions for grassland growth in NWA and NA where the majority of cropland-grassland sample pairs are collected. By contrast, the warmer and wetter NCSH and SSH regions are rich in cropland-forest and forest-grassland pairs. NWA situated in the most north-western China, has few cropland-forest pairs and thus no available extracted variables for cropland-forest (Fig. 6b).

From regional averaged difference for each pair in T2-ave, LAI, and albedo during summertime, we can explore the climatic effects of each vegetation conversion pairs over each region (Fig. 6b). As these pairs are close enough, their differences in temperature, LAI, and albedo can be regarded as the major contribution of land-cover conversions. Albedo and LAI are the two most important land surface properties which corporately affect the near-surface temperature. LAI and albedo show scattered pattern because of the heterogeneous spatial distribution of land-cover and tend to display the opposite impact on temperature among all regions. Decreasing albedo would increase the absorbed net radiation while LAI reduction dampens the cooling effect of ET, conjunctly warming the surface air. Croplands are represented with larger albedo and lower LAI than forests in all regions. Thus, other than the cooling T2-ave in NA due to the extreme large albedo, the other regions get larger warming effects of cropland than those of forest. Cropland and forest in NA are cooler than their surrounding grassland, in agreement with the results of Zhao et al. (2017). NEH featured with dense forest growth owns much higher LAI and lower albedo relative to their surrounding cropland (Fig. 6b upper). This results in an outstanding T2 increase and shows the stronger albedo warming impact than ET cooling over the high latitudinal areas. For forest-grassland samples, forest has larger LAI and smaller albedo than grass, leading to cooler T2 of forest than that of grassland. Temperature differences of cropland-grassland pairs are very small, indicating cropland and grassland have similar LAI and albedo except for in NWA where cropland exhibits significantly higher greening and LAI than those of grassland.

CRU annual mean temperature shows a weak warming trend from 2000 to 2015 with the highest T2-ave of 8.1 °C in 2015 (Fig. 7a). Comparisons of three vegetation conversions show consistent trends in temperature and biophysical property changes along year 2000, 2005, 2010, and 2015 but the magnitude varies with zones inter-annually (Fig. 7b).

Over three regions with larger pair amount for each vegetation conversion, the cropland-forest conversion, that is the conversion from forest to cropland, over NEH, NCSH

and SSH reveals comparable changes of T2 and biophysical properties despite the distinct differences of moisture and sunshine (Fig. 7b). In NEH, decreased warming of T2 for cropland-forest can be explained by the enhanced albedo and reduced LAI changes. While in the southern tropical SSH, a slight decline of T2 difference is found which is driven by a significantly increasing LAI differences and indicates a suppression of vegetation-induced local temperature changes under global warming. The other two vegetation conversions with higher uncertainties present more obvious heterogeneous characteristics over the selected climatic zones. Cropland-grassland pairs in NWA and NA show the same signs in albedo and LAI changes from 2000 to 2015 but opposite T2-ave variation, indicating the dominant LAI impact in NWA but albedo effect in NA (Fig. 7c). In addition, the changes in T2-max and T2-min of cropland-grassland pairs in all regions have completely opposite signs. This suggests that the type of cropland and grassland over NWA and NA have obvious differences in their specific heat capacity which could determine the warming efficiency with absorbing the same amount of energy. Forest-grassland samples in NEH and NWA have similar changes in LAI and albedo with a decreasing trend from 2000 to 2015, and so are the T2-ave differences (Fig. 7d). NCSH region shows no consistent changes of T2 due to the limited sample pairs. Thus, regional variations in land-cover type play crucial roles in determining local temperature differences and no evident influence of the background climate are found among the vegetation induced temperature changes.

### 3.3 Latitudinal variations of three vegetation conversions

Sunshine varies following latitudinal changes as it influences the incident shortwave radiation which is closely associated with the changes of the surface temperature (Lee et al. 2011). Moreover, vegetation living on the photosynthesis process displays heterogeneous distribution of types along latitude. Figure 8 shows that the changes of T2-max are negatively correlated with that of LAI for nearly all conversion types below 30° N. The strong correlation suggests that the LAI may be the main reason accounting for the T2-max changes along the latitude, particularly for cropland-grassland pairs. Interestingly, there is also a positive correlation between changes in temperature and albedo contradicting to the relationship between LAI and temperature below 30° N for cropland-forest and forest-grassland pairs. This indicates that the albedo changes are also induced by LAI and further confirm the driving role of LAI in modulating temperature changes. Vegetation type with larger LAI tends to have stronger ET and smaller albedo which causes a cooling and warming effect, respectively. However, the former impact overwhelms the latter, resulting in a net cooling effect and



**Fig. 7** a Annual CRU temperature changes in China from 2000 to 2015, the red line is the linear trend over this period; differences of monthly T2-ave, T2-max, T2-min, Albedo, and LAI on b cropland and forest (cropland–forest) over NEH, NCSH, and SSH regions, c

cropland and grassland (cropland–grassland) over NWA, NA, and NH regions, (d) forest and grassland (forest–grassland) over NEH, NWA, and NCSH regions for 2000, 2005, 2010, and 2015

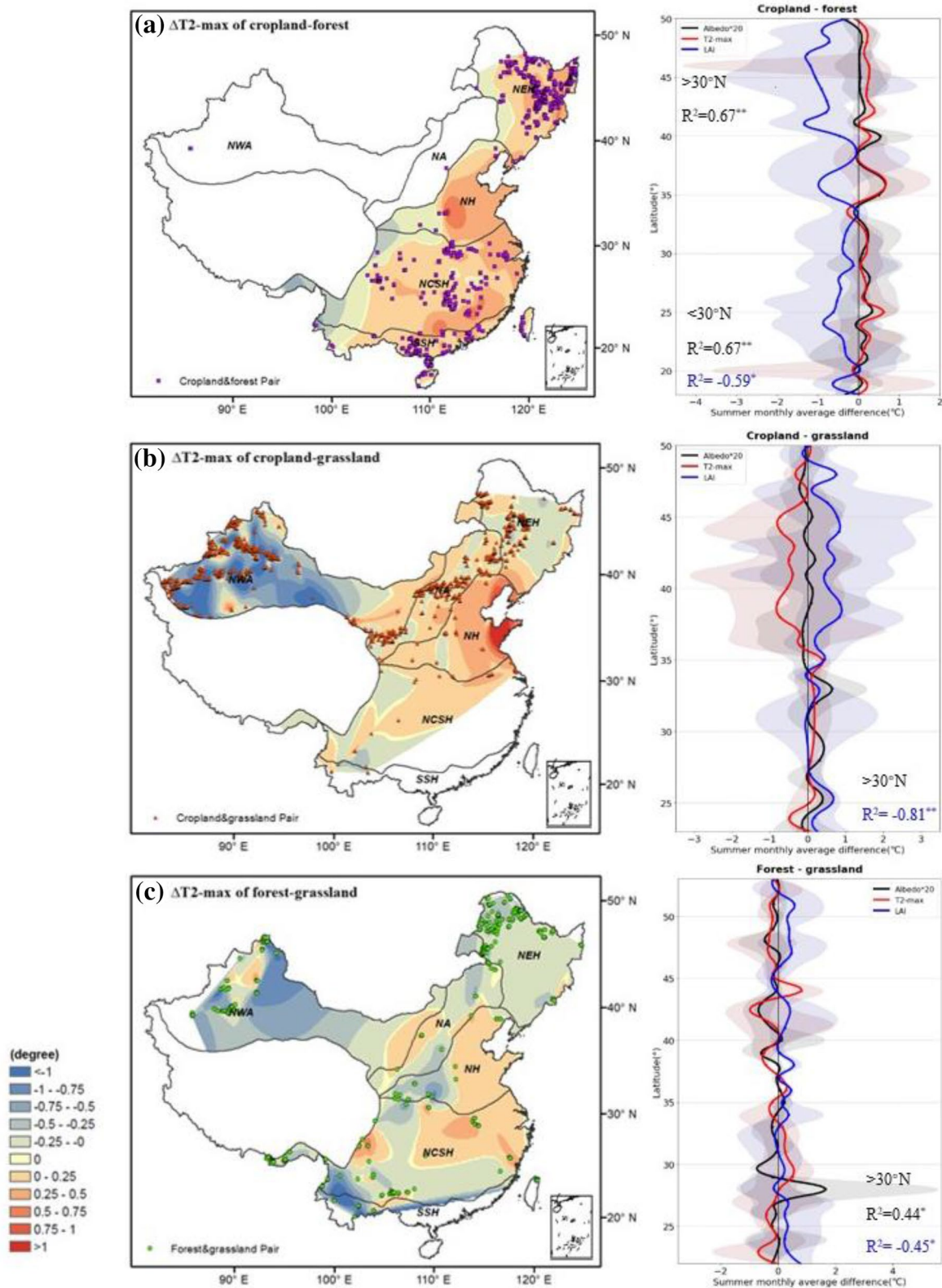


**Fig. 8** Latitudinal variation of summer (June, July, and August) monthly T2-max (red line), LAI (blue line) and albedo (black line) differences on **a** cropland and forest (cropland–forest), **b** cropland and grassland (cropland–grassland), **c** forest and grassland (forest–grassland), which are fitted by 1° latitude bin averaged values. The

shadow areas in light black, red, and blue are their corresponding ranges of pair differences. Correlations between T2-max and albedo are marked in black while T2-max and LAI are in blue with an asterisk meaning significance at 0.05 level and two meaning at 0.01 level

thus getting a negative correlation between T2 and LAI. The dominated LAI impact is much stronger in higher latitudes such as NH and NEH where the temperature is not sensitive to albedo because of relatively less sunlight duration. By contrast, the temperature is more sensitive to albedo in lower latitudes, and the compensating effect between ET and albedo results in small temperature changes.

Cropland–forest pairs mainly exist in 18°–35° N and 40°–50° N and indicate that cropland is warmer than forest. Forest has lower albedo and higher LAI than cropland, resulting in a net cooling from stronger forest ET (Fig. 8a). From south to north, the dense forest cover over northeast China produces higher ET than those of southern regions, which exceeds the intensive albedo induced warming, leading to a net cooling effect on climate in high latitudinal regions, consistent with Li et al. (2016). In total, summer cropland is warmer than their surrounding forest by 0.14 °C on average over the region of NEH, NCSH, and SSH. Grassland shows a more intensive heating of air temperature by 0.3 °C than croplands (Fig. 8b). T2-max differences for cropland–grassland pairs and cropland–forest show an inverse sign, illustrating grassland ranking the most warming efficient vegetation followed by cropland and forest in temperate and boreal regions. As sparse pairs are available for forest and grass in all regions except for NEH, the variations among T2, albedo, and LAI demonstrate slight significant correlations and albedo and LAI jointly lead to a majority of cooling on T2 by 0.09 °C on average (Fig. 8c).

### 3.4 Differences of temperature responses between modelling simulation and observation

Note that the different temperature responses between model and observation results could partly be because the coupled model simulation considered atmospheric feedback between land surface and atmosphere, which are particularly strong during the warm season (Winckler et al. 2017; Devaraju

et al. 2018). Therefore, average T2 changes are calculated and compared for the three land-cover pairs, cropland–forest, cropland–grassland, forest–grassland, over various regions based on both simulation results and observational datasets (Fig. 9). The largest inconsistencies occur in cropland–forest pairs with totally opposite summer T2 changes in NH, NCSH&SSH, and NEH&NA, indicating a very strong land–atmosphere interaction in climate simulation in warm season for cropland and forest (Fig. 9a). Cropland tends to have higher temperature than forest from locally aspect as deforestation to cropland results in higher albedo and less ET. However, this will be changed after considering the atmospheric circulation and cloud impacts as simulated T2 of cropland is much lower than that of forest, agreeing with most modelling studies which revealed that deforestation leads to cooling effect from historical land-use and land-cover over middle and high latitudes (Lejeune et al. 2017; Chen and Dirmeyer 2020). Pair-sites cropland–forest consists of nearby samples, which fulfils the assumption that they share similar background conditions. Thus, this comparison illustrates that background climate from the model simulation can overwhelm the local warming effects represented in the paired cropland–forest.

Obvious regional and seasonal influences of atmospheric feedbacks may be found in cropland–grassland as summer T2 changes in NH and NCSH&SSH locating in southern China show discrepancies between observed and simulated results (Fig. 9b). Cropland warms the local temperature than grassland in summer but cools the climate in winter from the pair-site stations. The warming effects can be totally offset by the atmosphere cooling impact over the whole southern region due to strong ET (Fig. 4b) and LHF occurrence (Fig. 5c). Northern regions such as NWA and NEH&NA show uniform variations but large differences in magnitudes for cropland–grassland as local effects are several times as the simulated changes especially in NWA (Fig. 9c). Regional changes of forest–grassland induced temperature are highly

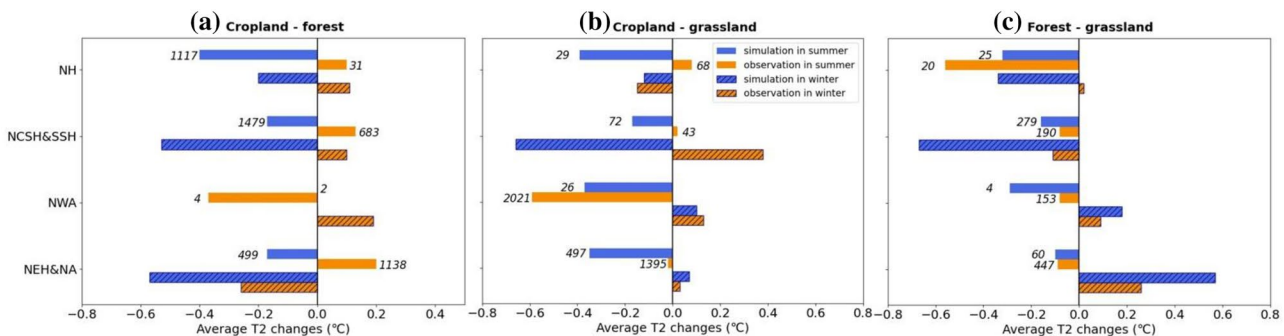


**Fig. 9** Average T2 changes with three vegetation conversion pairs **a** cropland–forest; **b** cropland–grassland; **c** forest–grassland over NH, NCSH&SSH, NWA, and NEH&NA based on model simulation (blue) and observation (orange). Blue bars are calculated using simu-

lated result while orange bars are from observation data. Bars with shadow lines are from winter data. Numbers following each simulation and observation bar are the amount of conversion pairs extracted within each region

consistent except for the winter variation in NH. This slight disagreement might be resulted from different spatial resolution (i.e., 20 km for simulated climatic changes and 1 km for observation). In summer, cooling effects of forest from higher LAI and enhanced ET exceeding grassland over NH and NCSH&SSH demonstrate uniformed decreasing on T2 changes in both simulation and observational results. Opposite warming impacts are found for forest in winter over northern China. In general, most incompatible changes for simulation and observational cases are for cropland-forest and cropland-grassland, which may come from either the atmospheric feedback of coupled simulation or the uncertainty of the land surface model as cropland is regarded as only one type in the land cover input of the model which would reduce the accuracy of the LAI and albedo calculation of the land surface model. However, it is difficult for the regional climate model to eliminate the atmosphere feedback impact through land-cover sub-grid experiments as those for global models carried out by Malyshev et al. (2015) and Chen and Dirmeyer (2020). Further improvements are needed for regional climate models to distinguish their local and non-local effects of land-cover.

## 4 Summary and conclusions

Land-cover change influences biophysical processes of energy and moisture exchange, which are essential and crucial to interactions between anthropogenic activities and the atmosphere. The surface properties among cropland, forest, and grassland affect the near-surface temperature to a wide spatial-temporal variation (e.g., Wickham et al. 2012; Zhao and Jackson 2014). In this study, comparisons are implemented between regional WRF modelling results and observational datasets in terms of the T2 changes caused by three vegetation conversion pairs (cropland-forest, cropland-grassland, and forest-grassland) to investigate roles of vegetation and the differences in the mechanism of climate model and actual in-situ measurements and satellite monitoring. Local and regional influences of LAI, albedo and energy partitioning between LHF and SHF are discussed in relation to T2 changes. Characteristics of each vegetation conversion along with their distribution on regional and latitudinal variation are highlighted through changes in net radiation and latent heat loss and their effects on temperature. WRF simulation with massive vegetation area changes between potential land-cover and historical anthropogenic land-cover demonstrates stronger ET effect on summer T2 and decreased SHF on winter T2, resulting in an overall cooling of 0.2 °C in summer and 0.31 °C in winter, which are in agreement with the deforestation impact from Ge et al. (2014) and Li et al. (2016). However, observational datasets show higher boreal and temperate T2 of cropland than those

of forest and grassland, which are inconsistent with Zhang and Liang (2018) and Huang et al. (2018b) in cropland-forest but consistent in cropland-grassland interactions, which may result from the different data sources. Grassland warming effects than forest is similar with those mentioned by Zhao et al. (2017). Latitudinal temperature changes using in-situ pairs indicate the dominant cooling effect of latitudinal LAI changes. Overall, ET as the driving factor in summer T2 changes displays stronger regional impact on modelling results than that of observations between cropland and forest, which may be originated from the inner parameterize vegetation phenology and biophysical properties in WRF. This can also be relevant to the atmospheric feedback impact on crop-forest and crop-grassland effects of which the temperature responses are opposite between modelling and observational datasets and should be further explored by using more detailed regional modelling such as sub-grid land-use change simulations.

This study not only reviews research on vegetation induced regional climate change but also investigates the actual case comparison between relative high-resolution simulation and observational datasets over heterogeneous regions, contributing to reveal deeper differences in modelling mechanism and in-situ changes and promote local and regional climate changes. However, as indicated by Zhao and Jackson (2014) and Zhu and Zeng (2017), forest type such as needleleaf and broadleaf within different climate zones could present opposite influences on the surface temperature, should be considered in detail instead of combining them into one forest type. Seasonal changes including spring and autumn (Zhu and Zeng 2015) making an essential contribution to annual warming and cooling need to be evaluated to improve the accuracy of model parameterization on the relationship between vegetation and climate.

**Supplementary Information** The online version contains supplementary material available at <https://doi.org/10.1007/s00382-021-06028-9>.

**Acknowledgements** We thank the editor and two anonymous reviewers whose insightful comments lead to a significant improvement of the manuscript. We greatly appreciate Dr. Gang Li from School of Geospatial Science and Engineering, Sun Yat-sen University for providing the computational resources to support this research. This research was funded by the Fundamental Research Funds for the Central Universities, Sun Yat-sen University, the National Natural Science Foundation of China (Grant no. 41871029) and the National Key R&D Program of China (2019YFC1510400). Zhen Liu was supported by the Institute for Basic Science (IBS), Republic of Korea, under IBS-R028-D1. The appointment of M. Luo at Sun Yat-sen University is partially supported by the Pearl River Talent Plan of Guangdong Province, China (2017GC010634).

**Availability of data and material** FNL data are available upon request from the website (<http://rda.ucar.edu/datasets/ds083.2/>). The CRU observations can be download freely from the Climatic Research Unit at the University of East Anglia (<http://www.cru.uea.ac.uk/cru/data/hrg/>). CLUM land-cover data can be download freely from the

Resource and Environment Science and Data Center of Chinese Academy of Sciences (<https://www.resdc.cn/>). The albedo and LAI dataset are download on request from Copernicus Climate Data Store (<https://cds.climate.copernicus.eu/cdsapp#!/home>). The daily meteorological observations are available from the China Meteorological Data Service Centre (<http://data.cma.cn/en>).

## Declarations

**Conflict of interest** The authors declare that they have no competing interests.

## References

- Alkama R, Cescatti A (2016) Climate change: biophysical climate impacts of recent changes in global forest cover. *Science* (80-) 351:600–604. <https://doi.org/10.1126/science.aac8083>
- Argüeso D, Evans JP, Fita L, Bormann KJ (2014) Temperature response to future urbanization and climate change. *Clim Dyn* 42:2183–2199. <https://doi.org/10.1007/s00382-013-1789-6>
- Brovkin V, Boysen L, Arora VK et al (2013) Effect of anthropogenic land-use and land-cover changes on climate and land carbon storage in CMIP5 projections for the twenty-first century. *J Clim* 26:6859–6881. <https://doi.org/10.1175/JCLI-D-12-00623.1>
- Cao Q, Yu D, Georgescu M, Wu J (2018) Substantial impacts of landscape changes on summer climate with major regional differences: the case of China. *Sci Total Environ* 625:416–427
- Chen F, Dudhia J (2001) Coupling an advanced land surface—hydrology model with the Penn State – NCAR MM5 modeling system. Part I: model implementation and sensitivity. *Mon Weather Rev* 56:585. [https://doi.org/10.1175/1520-0493\(2001\)129%3c0569:caalsh%3e2.0.co;2](https://doi.org/10.1175/1520-0493(2001)129%3c0569:caalsh%3e2.0.co;2)
- Chen L, Frauenfeld OW (2016) Impacts of urbanization on future climate in China. *Clim Dyn* 47:345–357
- Chen L, Dirmeyer PA (2020) Reconciling the disagreement between observed and simulated temperature responses to deforestation. *Nat Commun* 11(1):202–202
- Chen C, Park T, Wang X et al (2019) China and India lead in greening of the world through land-use management. *Nat Sustain* 2:122–129. <https://doi.org/10.1038/s41893-019-0220-7>
- Davin EL, de Noblet-Ducoudre N (2010) Climatic impact of global-scale deforestation: radiative versus nonradiative processes. *J Clim* 23:97–112. <https://doi.org/10.1175/2009JCLI3102.1>
- De Noblet-Ducoudré N, Boisier JP, Pitman A et al (2012) Determining robust impacts of land-use-induced land cover changes on surface climate over North America and Eurasia: results from the first set of LUCID experiments. *J Clim* 25:3261–3281. <https://doi.org/10.1175/JCLI-D-11-00338.1>
- Devaraju N, de Noblet-Ducoudre N, Quesada B, Bala G (2018) Quantifying the relative importance of direct and indirect biophysical effects of deforestation on surface temperature and teleconnections. *J Clim* 31(10):3811–3829. <https://doi.org/10.1175/JCLI-D-17-0563.1>
- Dong N, Liu Z, Luo M et al (2019) The effects of anthropogenic land use changes on climate in China driven by global socio-economic and emission scenarios. *Earth's Future* 7:784–804. <https://doi.org/10.1029/2018EF000932>
- Feng JM, Wang YL, Ma ZG, Liu YH (2012) Simulating the regional impacts of urbanization and anthropogenic heat release on climate across China. *J Clim* 25:7187–7203. <https://doi.org/10.1175/JCLI-D-11-00333.1>
- Findell KL, Shevliakova E, Milly PCD, Stouffer RJ (2007) Modeled impact of anthropogenic land cover change on climate. *J Clim* 20:3621–3634. <https://doi.org/10.1175/JCLI4185.1>
- Forzieri G, Alkama R, Miralles DG, Cescatti A (2017) Satellites reveal contrasting responses of regional climate to the widespread greening of Earth. *Science* (80-) 356:1180–1184. <https://doi.org/10.1126/science.aal1727>
- Ge Q, Zhang X, Zheng J (2014) Simulated effects of vegetation increase/decrease on temperature changes from 1982 to 2000 across the Eastern China. *Int J Climatol* 34:187–196. <https://doi.org/10.1002/joc.3677>
- Ge J, Guo W, Pitman AJ, Kauwe MGD, Chen X, Fu C (2019) The nonradiative effect dominates local surface temperature change caused by afforestation in China. *J Clim* 32(14):4445–4471
- Guo WD, Wang XQ, Sun JN, Ding AJ, Zou J (2016) Comparison of land–atmosphere interaction at different surface types in the mid-to lower reaches of the yangtze river valley. *Atmos Chem Phys* 16(15):1–42
- Harris I, Jones PD, Osborn TJ, Lister DH (2014) Updated high-resolution grids of monthly climatic observations—the CRU TS3.10 Dataset. *Int J Climatol* 34:623–642. <https://doi.org/10.1002/joc.3711>
- Huang L, Zhai J, Liu J, Sun C (2018a) The moderating or amplifying biophysical effects of afforestation on CO<sub>2</sub>-induced cooling depend on the local background climate regimes in China. *Agric for Meteorol* 260–261:193–203. <https://doi.org/10.1016/j.agrfor.2018.05.020>
- Huang L, Zhai J, Sun CY, Liu JY, Ning J, Zhao GS (2018b) Biogeophysical forcing of land-use changes on local temperatures across different climate regimes in China. *J Clim* 31(17):7053–7068
- Kusaka H, Kimura F (2004) Thermal effects of urban canyon structure on the nocturnal heat island: numerical experiment using a mesoscale model coupled with an urban canopy model. *J Appl Meteorol* 43:1899–1910. <https://doi.org/10.1175/JAM2169.1>
- Lee X, Goulden ML, Hollinger DY et al (2011) Observed increase in local cooling effect of deforestation at higher latitudes. *Nature* 479:384–387. <https://doi.org/10.1038/nature10588>
- Lejeune Q, Seneviratne SI, Davin EL (2017) Historical land-cover change impacts on climate: comparative assessment of LUCID and CMIP5 multimodel experiments. *J Clim* 30(4):1439–1459
- Li Y, Zhao M, Motesharrei S et al (2015) Local cooling and warming effects of forests based on satellite observations. *Nat Commun*. <https://doi.org/10.1038/ncomms7603>
- Li Y, De Noblet-Ducoudré N, Davin EL et al (2016) The role of spatial scale and background climate in the latitudinal temperature response to deforestation. *Earth Syst Dyn* 7:167–181. <https://doi.org/10.5194/esd-7-167-2016>
- Liu J, Zhang Z, Xu X et al (2010) Spatial patterns and driving forces of land use change in China during the early 21st century. *J Geogr Sci* 20:483–494. <https://doi.org/10.1007/s11442-010-0483-4>
- Liu J, Kuang W, Zhang Z et al (2014) Spatiotemporal characteristics, patterns and causes of land use changes in China since the late 1980s. *Acta Geogr Sin* 69:3–14. <https://doi.org/10.11821/dlxb201401001>
- Ma W, Jia G, Zhang A (2017) Multiple satellite-based analysis reveals complex climate effects of temperate forests and related energy budget. *J Geophys Res* 122(7):3806–3820
- Mahmood R, Pielke RA, Hubbard KG et al (2014) Land cover changes and their biogeophysical effects on climate. *Int J Climatol* 34:929–953. <https://doi.org/10.1002/joc.3736>
- Malyshev S, Shevliakova E, Stouffer RJ, Pacala SW (2015) Contrasting local versus regional effects of land-use-change-induced heterogeneity on historical climate: analysis with the GFDL earth system model. *J Clim* 28:5448–5469. <https://doi.org/10.1175/JCLI-D-14-00586.1>



- National Centers for Environmental Prediction/National Weather Service/NOAA/U.S. Department of Commerce (2000) NCEP FNL Operational Model Global Tropospheric Analyses, continuing from July 1999, Research Data Archive at the National Center for Atmospheric Research, Computational and Information Systems Laboratory. <https://doi.org/10.5065/D6M043C6>
- NCAR Nc for AR (2016) ARW Modelling System UserGuide V.3 vol 3. Book 408. <https://doi.org/10.5065/D68S4MVH>
- Peng S-S, Piao S, Zeng Z, Ciais P, Zhou L, Li LZ, Zeng H (2014) Afforestation in China cools local land surface temperature. *Proc Natl Acad Sci USA* 111(8):2915–2919
- Peng S, Ding Y, Liu W, Li Z (2019) 1km monthly temperature and precipitation dataset for China from 1901 to 2017. *Earth Syst Sci Data* 11:1931–1946. <https://doi.org/10.5194/essd-11-1931-2019>
- Pielke RA, Pitman A, Niyogi D et al (2011) Land use/land cover changes and climate: Modeling analysis and observational evidence. *Wiley Interdiscip Rev Clim Change* 2:828–850
- Pitman AJ, Avila FB, Abramowitz G et al (2011) Importance of background climate in determining impact of land-cover change on regional climate. *Nat Clim Change* 1:472–475. <https://doi.org/10.1038/nclimate1294>
- Ramankutty N, Foley JA (1999) Estimating historical changes in global land cover: Croplands from 1700 to 1992. *Glob Biogeochem Cycles* 13:997–1027. <https://doi.org/10.1029/1999GB900046>
- Schaaf CB, Gao F, Strahler AH et al (2002) First operational BRDF, albedo nadir reflectance products from MODIS. *Remote Sens Environ* 83:135–148. [https://doi.org/10.1016/S0034-4257\(02\)00091-3](https://doi.org/10.1016/S0034-4257(02)00091-3)
- Shen W, Li M, Huang C, He T, Tao X, Wei A (2019) Local land surface temperature change induced by afforestation based on satellite observations in Guangdong plantation forests in China. *Agric for Meteorol* 276:107641
- Skamarock WC, Wang W, Klemp JB, Dudhia J, Gill DO, Barker DM, Powers JG (2008) 2005: a description of the advanced research WRF Version 3. NCAR Tech Note, pp 488–494
- Wang X, Guo W, Qiu B, Liu Y, Sun J, Ding A (2016) Quantifying the contribution of land use change to surface temperature in the lower reaches of the Yangtze River. *Atmos Chem Phys* 17(8):4989–4996
- Wang L, Lee X, Schultz N, Chen S, Wei Z, Fu C, Lin G (2018) Response of surface temperature to afforestation in the Kubuqi Desert, Inner Mongolia. *J Geophys Res* 123(2):948–964
- Wickham JD, Wade TG, Riitters KH (2012) Comparison of cropland and forest surface temperatures across the conterminous United States. *Agric for Meteorol* 166–167:137–143. <https://doi.org/10.1016/j.agrformet.2012.07.002>
- Winckler J, Reick CH, Pongratz J (2017) Robust identification of local biogeophysical effects of land-cover change in a global climate model. *J Clim* 30:1159–1176. <https://doi.org/10.1175/JCLI-D-16-0067.1>
- Xu Z, Mahmood R, Yang ZL et al (2015) Investigating diurnal and seasonal climatic response to land use and land cover change over monsoon Asia with the community earth system model. *J Geophys Res* 120:1137–1152. <https://doi.org/10.1002/2014JD022479>
- Zeng Z, Piao S, Li LZ et al (2017) Climate mitigation from vegetation biophysical feedbacks during the past three decades. *Nat Clim Chang* 7:432–436. <https://doi.org/10.1038/nclimate3299>
- Zhang Y, Liang S (2018) Impacts of land cover transitions on surface temperature in China based on satellite observations. *Environ Res Lett*. <https://doi.org/10.1088/1748-9326/aa9e93>
- Zhang J, Cha DH, Lee DK (2009) Investigating the role of MODIS Leaf Area Index and vegetation-climate interaction in regional climate simulations over Asia. *Terr Atmos Ocean Sci* 20:377–393. [https://doi.org/10.3319/TAO.2008.04.03.01\(A\)](https://doi.org/10.3319/TAO.2008.04.03.01(A))
- Zhang M, Lee X, Yu G et al (2014) Response of surface air temperature to small-scale land clearing across latitudes. *Environ Res Lett*. <https://doi.org/10.1088/1748-9326/9/3/034002>
- Zhao K, Jackson RB (2014) Biophysical forcings of land-use changes from potential forestry activities in North America. *Ecol Monogr* 84:329–353. <https://doi.org/10.1890/12-1705.1>
- Zhao W, Hu Z, Li S et al (2017) Comparison of surface energy budgets and feedbacks to microclimate among different land use types in an agro-pastoral ecotone of northern China. *Sci Total Environ* 599–600:891–898. <https://doi.org/10.1016/j.scitotenv.2017.04.200>
- Zhu J, Zeng X (2015) Comprehensive study on the influence of evapotranspiration and albedo on surface temperature related to changes in the leaf area index. *Adv Atmos Sci* 32:935–942. <https://doi.org/10.1007/s00376-014-4045-z>
- Zhu J, Zeng X (2017) Influences of the seasonal growth of vegetation on surface energy budgets over middle to high latitudes. *Int J Climatol* 37:4251–4260. <https://doi.org/10.1002/joc.5068>
- Zhu K (1931) China climate regionalism. *J Meteorol Inst* 1: 1–11. (in Chinese)
- Zhu B et al (1962) Chinese meteorology. Chinese Science Press (in Chinese)

**Publisher's Note** Springer Nature remains neutral with regard to jurisdictional claims in published maps and institutional affiliations.